frontiers | Frontiers in Built Environment

TYPE Original Research
PUBLISHED 31 May 2024
DOI 10.3389/fbuil.2024.1386803

OPEN ACCESS

EDITED BY
Krishna Kumar,
The University of Texas at Austin, United States

REVIEWED BY
Christos Vrettos,
University of Kaiserslautern, Germany
Rui Chen,
Harbin Institute of Technology, Shenzhen, China

*CORRESPONDENCE
Diane Moug,
dmoug@pdx.edu

RECEIVED 16 February 2024
ACCEPTED 24 April 2024
PUBLISHED 31 May 2024

CITATION
Moug D, Huffman A and DeJong JT (2024), Investigation of piezocone dissipation test interpretation in clay accounting for vertical and horizontal porewater pressure dissipation with a large deformation axisymmetric penetration model.
Front. Built Environ. 10:1386803.
doi: 10.3389/fbuil.2024.1386803

Investigation of piezocone dissipation test interpretation in clay accounting for vertical and horizontal porewater pressure dissipation with a large deformation axisymmetric penetration model

Diane Moug[1]*, Andrew Huffman[1] and Jason T. DeJong[2]

[1]Civil and Environmental Engineering, Portland State University, Portland, OR, United States, [2]Civil and Environmental Engineering, University of California, Davis, Davis, CA, United States

The piezocone (CPTu) dissipation test is used to characterize how the applied load from the penetrating cone is distributed between the soil and pore fluid during both penetrometer advancement and when penetration is paused. The coefficient of consolidation is often estimated from CPTu dissipation tests by interpreting the rate of excess porewater pressure (Δu) decay to static conditions during a pause in cone penetration. Most CPTu dissipation test interpretation methods are based on Terzaghi consolidation theory for Δu dissipation at the cone shoulder (u_2 position) or cone face (u_1 position) and assume that radial Δu dissipation dominates the response. However, several recent studies show that vertical Δu migration does contribute to the response. This study uses a large deformation direct axisymmetric cone penetration model to characterize the soil-water mechanical response during CPTu dissipation tests, and in particular, the role of vertical Δu dissipation on the response at the u_1 and u_2 positions. Large deformations around the penetrating cone are accommodated with an Arbitrary Lagrangian Eulerian approach. Soil behavior is modeled with the MIT-S1 constitutive model calibrated for Boston blue clay (BBC) soil behavior. Δu dissipation following undrained cone penetration is simulated with coupled consolidation for BBC with over-consolidation ratios (OCR) of 1, 2, and 4 and a range of hydraulic conductivity anisotropy. The simulated u_1 and u_2 dissipation responses are presented to study how they are affected by OCR and hydraulic conductivity anisotropy. A correction factor is recommended to account for hydraulic conductivity anisotropy when interpreting the horizontal coefficient of consolidation from CPTu dissipation tests.

KEYWORDS

cone penetration testing, dissipation testing, ALE, large deformations, finite deformation, overconsolidated clay, coefficient of consolidation

1 Introduction

The piezocone (CPTu) dissipation test is used in geotechnical engineering and environmental engineering to characterize how the applied load from the penetrating cone is distributed between the soil and pore fluid during both penetrometer advancement and when penetration is paused. The test is performed by pausing cone penetration and monitoring excess porewater pressure (Δu) dissipation with time at discrete locations on the cone penetrometer. The soil coefficient of consolidation and hydraulic conductivity, which the CPTu dissipation test interprets, control the rate at which the porewater pressure enables stress transfer from the pore fluid to the soil skeleton.

Many commonly used CPTu dissipation interpretation methods assume that radial Δu dissipation dominates the measured response (e.g., Teh and Houlsby, 1991; Burns and Mayne, 1998), and therefore, interpretation yields estimates for the horizontal coefficient of consolidation (c_h) and the horizontal soil permeability (k_h). However, subsequent studies note that vertical Δu migration contributes to the CPTu u_2 dissipation test response, including Chai et al. (2014), Agaiby and Mayne (2018), and Tsegaye (2021). In particular, Agaiby and Mayne (2018) note that the interpreted coefficient of consolidation reflects hydraulic properties in both vertical and horizontal directions and, therefore, term the interpreted value to be c_{vh}. Therefore, c_h may be over or underestimated depending on the soil's vertical hydraulic conductivity (k_v) and hydraulic conductivity anisotropy (i.e., k_h/k_v). Although the influence of k_v and vertical Δu migration is recognized, no current methods for CPTu dissipation test interpretation explicitly account for these properties when interpreting CPTu dissipation tests.

Numerical investigations into porewater pressure dissipation following undrained penetration are one of the primary tools for understanding the mechanics of the CPTu dissipation test and developing and validating methods to interpret the test results. These investigations include indirect and direct approaches to simulate cone penetration. Indirect methods capture cone penetration loading as a cylindrical or spherical cavity expansion problem (e.g., Burns and Mayne, 1998; Imre et al., 2010). These are relatively simple approaches that can often capture Δu distributions around the cone with closed-form equations; however, the full loading condition from the penetrating cone is not captured, and porewater pressure migration is limited to the radial direction only. Direct penetration models simulate the full penetration loading condition on the surrounding soil and allow porewater pressure migration to occur vertically and radially. However, continuum methods (i.e., finite element or finite difference models) must accommodate large soil deformations around the penetrating cone, or mesh entanglement and other numerical errors will occur before reaching steady-state penetration conditions. Therefore, numerical techniques must be implemented to accommodate these large deformations. Continuum direct penetration models to study CPTu dissipation tests have been performed with the strain path method (Teh and Houlsby, 1991), a smooth cone-soil interface (Abu-Farskah et al., 2003), the press-replace method (Lim et al., 2019), the ABAQUS non-linear geometry option (Ansari et al., 2014; Deng et al., 2023), arbitrary Lagrangian Eulerian (ALE) techniques (Chai et al., 2012; Mahmoodzadeh et al., 2014; Liu et al., 2022), and material point methods (Ceccato and Simonini, 2016). These previous numerical dissipation studies used simple soil models such as Mohr Coulomb or modified Cam clay that do not fully capture the response of undrained clay to cone penetration loading, as shown in Moug et al. (2019).

Of the above studies, only Abu-Farskah et al. (2003) and Lim et al. (2019) studied the role of k_h/k_v during CPTu dissipation; the two studies yielded conflicting results. Abu-Farskah et al. (2003) found that k_h/k_v does affect the u_1 and u_2 dissipation responses comparing simulations of $k_h = k_v, k_h = 10k_v$ and $k_v = 10k_h$; while Lim et al. (2019) found no effect of k_h/k_v on the u_2 dissipation curve. This study addresses the knowledge gap regarding the contribution of vertical porewater pressure dissipation when interpreting c_h by elucidating the role of k_h/k_v on CPTu dissipation tests and how k_h/k_v should be considered for c_h interpretation.

This study uses a direct, axisymmetric cone penetration model, ALE techniques, and an advanced constitutive model to investigate soil-water interactions during CPTu dissipation. The direct axisymmetric cone penetration model is implemented in the finite difference program FLAC and accommodates large deformations around the penetrating cone with a user-implemented ALE algorithm. An advanced elastoplastic bounding surface constitutive model, MIT-S1 (Pestana and Whittle, 1999), is calibrated for Boston blue clay (BBC) to capture anisotropic saturated clay behavior. This numerical model, specifically the combination of a large deformation direct penetration simulation and the use of a complex anisotropic soil model, differs from previous numerical studies of CPTu dissipation since it uses a direct penetration model that can capture the full loading condition around the penetrating cone, and can capture the anisotropic shear strength behavior and shear-induced Δu of saturated clay. Therefore, this numerical study is a step forward to improve theoretical understanding of piezocone dissipation tests in saturated clay. This study investigates the role of k_v and k_h/k_v during piezocone dissipation tests. Specifically, this study examines how k_h/k_v affects the dissipation responses at the cone tip (u_1 position) and the cone shoulder (u_2 position) to suggest an approach to estimate c_h and c_v that accounts for vertical Δu migration. CPTu dissipation following undrained penetration is examined for BBC with k_h/k_v ranging from 1 to 10. Simulations are performed for undrained penetration in saturated clay with OCR of 1, 2, and 4 to investigate if stress history affects the role of k_h/k_v during CPTu dissipation tests.

2 Axisymmetric piezocone penetration and dissipation model

A direct axisymmetric cone penetration model with ALE to accommodate large deformations was used to simulate CPTu dissipation following steady-state undrained penetration in clay. The simulations were performed using the explicit finite difference program FLAC 8.0 (Fast Lagrangian Analysis of Continua; Itasca 2016) with the MIT-S1 constitutive model (Pestana and Whittle, 1999; Pestana et al., 2002) calibrated for BBC. Penetration was simulated with initial OCR of 1, 2, and 4.

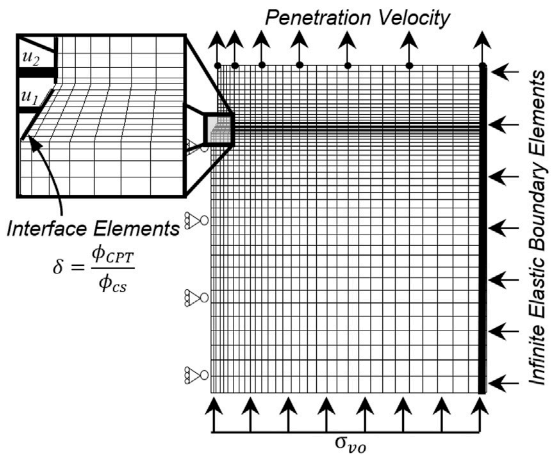

FIGURE 1
Penetration model geometry and boundary conditions.

2.1 Piezocone dissipation model

The axisymmetric model geometry simulates steady-state penetration at one depth in the soil column for a standard 10 cm^2 cone as shown in Figure 1. The model is initialized with stress and material properties for the "wished-in-place" condition at the depth of interest in the soil column. Cone geometry and conditions between the cone and soil are captured with Mohr-Coulomb interface elements that obey the Mohr-Coulomb friction condition. The interface coefficient of friction ($\delta = \phi_{cone}/\phi_{critical\ state}$) was set at 0.8, where 0.0 would represent a perfectly smooth cone and 1.0 would represent a perfectly rough cone. The stiffnesses of the shear and normal springs in these interface elements were set large enough that they had negligible effects on the solution (Itasca, 2016).

The penetration boundary conditions are specified for soil flowing upwards relative to a stationary cone; soil conceptually flows into the bottom of the model and exits at the top of the model. The *in-situ* vertical stress is applied across the bottom boundary, where this boundary is sufficiently far from the penetrating cone's zone of influence that the *in-situ* stress condition prevails. The right radial boundary is represented with an infinite elastic boundary condition and is sufficiently far from the penetrating cone to avoid boundary effects (Moug, 2017). The model dimensions are 37 cone diameters in the radial direction, 37 cone diameters below the cone tip, and 5 cone diameters above the cone shoulder. The cone penetration velocity is applied to all gridpoints across the top boundary, with adjustments made to the gridpoint adjacent to the cone shaft to accommodate friction at the soil-shaft interface. Penetration is then simulated until steady-state penetration resistance, and steady-state stress and Δu conditions around the penetrating cone are reached; for this work, steady-state stress and Δu distributions were considered to be achieved after 30 cone diameters of simulated penetration, which is consistent with Lu et al. (2004). Piezocone dissipation is simulated by first bringing the simulated penetration velocity to zero, then re-assigning hydraulic properties and monitoring Δu over the simulated time.

Groundwater seepage boundary conditions for simulated dissipation were a combination of no-flow, fixed porewater pressure, and leaky boundaries. A no-flow condition was assigned at the axisymmetric boundary (x = 0). *In-situ* static porewater pressures were fixed at the far radial boundary and the bottom horizontal boundary; these boundaries were far enough from the penetrating cone that $\Delta u = 0$ conditions prevailed. A leaky boundary was implemented at the top of the model to allow seepage flow across the boundary. The leaky boundary is assigned by assuming that the distance to $\Delta u = 0$ was the distance to the top of the water table and assuming a constant k_v over this distance.

2.2 ALE for large deformations cone penetration

Large deformations during simulated penetration are addressed with a user-implemented ALE algorithm that performs rezoning and remapping operations throughout simulated penetration (Moug et al., 2019). The user-defined ALE algorithm is coupled with FLAC's large deformation Lagrangian formulation to allow full penetration simulations and implementation with the MIT-S1 constitutive model. The ALE algorithm is implemented by simulating penetration for a time interval with FLAC's standard Lagrangian deformation formulation. The rezoning step takes place before significant deformation of the model zones occurs; the rezoning step resets the model geometry to the "undeformed" or original condition. The Eulerian remapping step then maps the model properties from the deformed model zones onto the undeformed model zones; this step is implemented in FLAC through a user-defined language according to the approach in Pember and Anderson (2001) and adapted for FLAC as described in Moug (2017). The Lagrangian, rezoning, and Eulerian remapping steps are continued in succession until steady-state cone penetration conditions are reached.

2.3 MIT-S1 Boston Blue clay calibration

The MIT-S1 constitutive model is a bounding surface plasticity model that can capture soil behavior from sedimentary clays to clean sands (Pestana and Whittle, 1999; Pestana et al., 2002). Jaeger (2012) initially implemented the version of MIT-S1 used in this study, with some minor modifications to the model. Additional modifications to the MIT-S1 implementation for the penetration model in FLAC are described in Moug (2017). Cone penetration and piezocone dissipation are simulated using the MIT-S1 model to accurately capture the effects of anisotropic s_u on the cone penetration problem, including the Δu distribution; Moug et al. (2019) demonstrated the role of s_u anisotropy on cone penetration tip resistance, stress distribution, and Δu distribution.

2.4 Hydraulic properties

The soil-water properties assigned to the FLAC model aimed to capture CPTu dissipation following undrained penetration. The fluid bulk modulus (K_{fluid}) was assigned to be at least 10 times larger than the soil skeleton bulk modulus or equal to $2x10^6$ kPa, whichever was smaller. This was numerically advantageous since it results in an incompressible K_{fluid} relative to the soil skeleton without compromising numerical

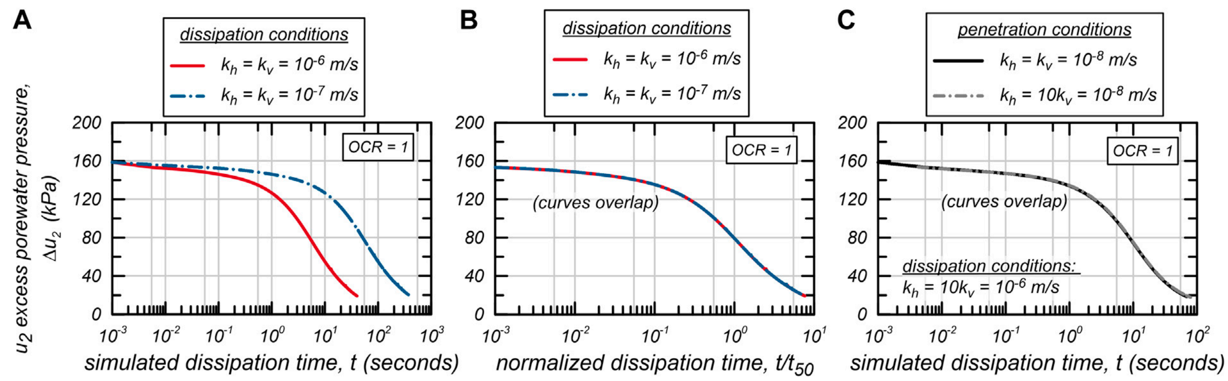

FIGURE 2
Simulated u_2 dissipation for OCR = 1: **(A)** Δu_2 versus simulated dissipation time for isotropic hydraulic conductivities, **(B)** Δu_2 versus simulated dissipation time normalized by t_{50} for isotropic hydraulic conductivities, and **(C)** Δu_2 versus simulated dissipation time from initial conditions for penetration in $k_h = k_v = 10^{-8}$ m/s and $k_h = 10k_v = 10^{-8}$ m/s clay.

efficiency as a large K_{fluid} can result in a small dynamic timestep and long simulation times. The model remained completely saturated throughout penetration and dissipation simulations.

The k_h and k_v values during cone penetration were assigned to capture a completely undrained penetration response according to the normalized penetration velocity (DeJong and Randolph, 2012). k_h and k_v values during CPTu dissipation were coupled to the mechanical response through the House (2012) relationship:

$$\frac{k_1}{k_2} = 10^{\frac{e_1 - e_2}{0.44}} \tag{1}$$

where this log-linear relationship between k and void ratio (e) was estimated with constant rate of strain consolidation tests on reconstituted BBC. k_1 represents the hydraulic conductivity at the void ratio e_1, and k_2 represents the hydraulic conductivity at the void ratio e_2. Similar relationships between e and k have been characterized by other researchers (e.g., Taylor, 1948; Dunn and Mitchell, 1984), however, the relationship in Eq. 1 was used for this study since it is specific to BBC. This relationship was incorporated into the CPTu dissipation simulations where k_h and k_v were updated throughout the simulations in response to simulated changes in e.

Simulated dissipation tests were performed for a range of k_h/k_v values where the lowest assigned hydraulic conductivities were $k_h = k_v = 10^{-7}$ m/s and the highest assigned hydraulic conductivities were $k_h = k_v = 10^{-6}$ m/s. These values of k_h and k_v are at least an order of magnitude higher than typical values for clayey soils (Kulhawy and Mayne, 1990). These higher-than-typical k values allowed this study to be performed without having exceedingly long simulation times due to low k values. The k values were found not to compromise the objectives of this study, as discussed in the following section.

2.5 Model validation

Dissipation was simulated with different k_h and k_v values from the same steady-state undrained penetration simulation for each OCR. This approach assumes that simulated Δu dissipation patterns depend on the initial Δu distribution and k anisotropy during dissipation.

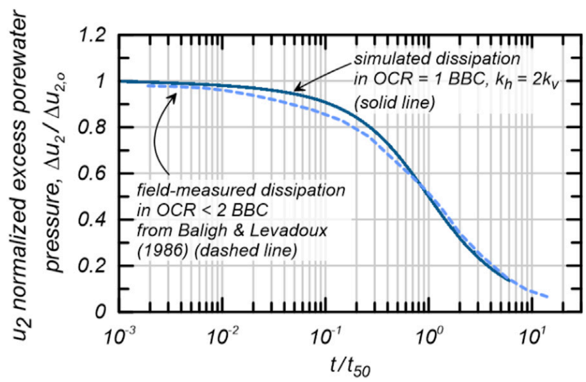

FIGURE 3
Comparison of simulated CPTu u_2 dissipation test in OCR = 1 BBC with Baligh and Levadoux (1986) CPTu field test in BBC.

Additionally, the approach assumes that dissipation is not affected by k_h/k_v values during penetration if undrained conditions prevail. Therefore, CPTu dissipation curves shift in time proportionally to changes to k when dissipation is simulated from the same initial state and with the same k_h/k_v. This assumption is validated in Figures 2A, B. Figure 2A compares the resulting dissipation curves for $k_h = k_v = 10^{-7}$ m/s and $k_h = k_v = 10^{-6}$ m/s as Δu_2 dissipation versus simulated time. Figure 2B compares the same curves as dissipation versus simulated time normalized by the time to 50% Δu dissipation (t_{50}) and shows that the curves normalize to an identical curve. Therefore, the assumption that Δu patterns during CPTu dissipation tests and the shape of CPTu curves are not affected by k magnitude during dissipation is reasonable for this study.

The assumption that the initial Δu distribution is unaffected if undrained penetration is simulated is further examined in Figure 2C. The figure shows two dissipation curves. One dissipation curve was simulated following steady-state penetration in soil with $k_h = k_v = 10^{-8}$ m/s, and the other following steady-state penetration in soil with $k_h = 10k_v = 10^{-8}$ m/s. Dissipation for both cases was simulated with $k_h = 10k_v = 10^{-6}$ m/s.

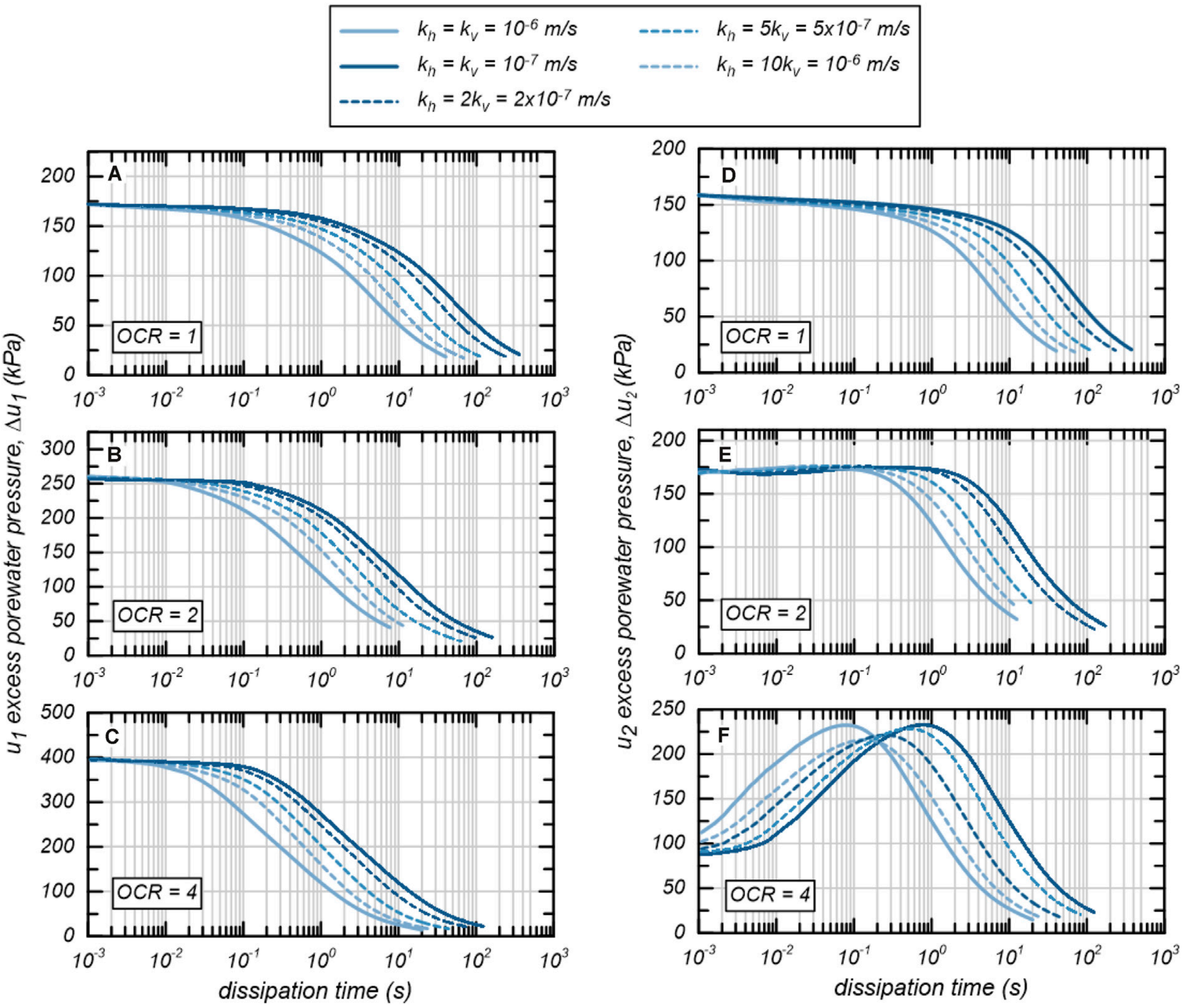

FIGURE 4
Simulated dissipation curves for OCR = 1, 2 and 4 with varying k_h/k_v at the u_1 **(A–C)** and u_2 **(D–F)** positions.

The resulting Δu_2 dissipation curves in Figure 2C are identical and validate the assumption that Δu dissipation patterns are unaffected by k_h/k_v during penetration provided k_h and k_v are small enough for undrained conditions to exist.

The CPTu simulations are further validated by comparing simulated results against a CPTu dissipation test performed in a BBC deposit. Figure 3 includes the published CPTu u_2 dissipation data from Baligh and Levadoux (1986) for BBC with an OCR less than 2 compared with simulated CPTu u_2 dissipation in BBC with OCR = 1. The tests are plotted as $\Delta u_2/\Delta u_{2,o}$ versus t/t_{50} to normalize the curves for stress conditions and c_h values. The close agreement indicates that the simulated CPTu dissipation tests in BBC can be used to study CPTu dissipation tests in normal clay.

3 Results of simulated piezocone dissipation

Dissipation following undrained steady-state cone penetration was simulated for BBC with OCR = 1, 2, and 4. The initial total vertical stress (σ_{vo}) and porewater pressure (u_o) for each case were 200 kPa and 100 kPa, respectively. Initial horizontal effective stress (σ'_{ho}) was established based on OCR and lateral at rest coefficient of effective stress ($K_0 = \sigma'_{ho}/\sigma'_{vo}$) for the MIT-S1 BBC calibration; K_0 values were 0.50, 0.60, and 0.80, for OCR = 1, 2, and 4, respectively. Dissipation was simulated for the initial k conditions: $k_h = k_v = 10^{-7}$ m/s, $k_h = 2k_v = 2x10^{-7}$ m/s, $k_h = 5k_v = 5x10^{-7}$ m/s, $k_h = 10k_v = 10^{-6}$ m/s, and $k_h = k_v = 10^{-6}$ m/s. As discussed above, k_h and k_v were updated throughout dissipation and coupled to the mechanical soil response.

3.1 Simulated dissipation at u_1 and u_2 positions

Dissipation over time was examined at the u_1 and u_2 positions. The u_1 dissipation curves show monotonic responses for all OCR conditions (Figures 4A–C), while the simulated u_2 dissipation curves result in monotonic or non-monotonic responses depending on initial OCR (Figures 4D–F). This is consistent with

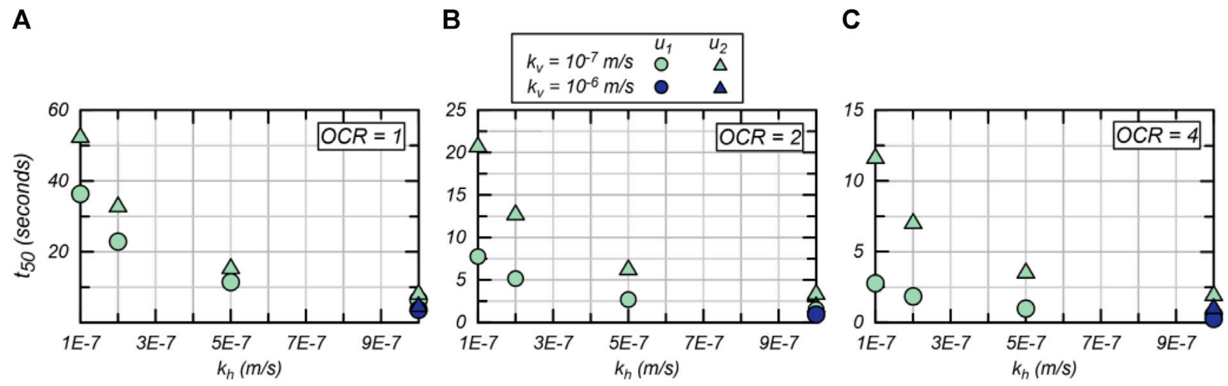

FIGURE 5
Simulated time to 50% of the maximum excess pore pressure at the u_1 and u_2 positions for **(A)** OCR = 1, **(B)** OCR = 2, and **(C)** OCR = 4.

published CPTu tests where monotonic responses prevail at the u_1 position regardless of whether a monotonic or non-monotonic response is observed at the u_2 position (e.g., Chen and Mayne, 1994; Sully et al., 1999; Finke et al., 2001). The simulated u_2 results show a monotonic dissipation response for OCR = 1, which is consistent with most piezocone dissipation tests following undrained penetration in normally consolidated soils (e.g., Burns and Mayne, 1998). The simulated results for OCR = 2 show a slightly non-monotonic u_2 response where the difference between $\Delta u_{2,o}$ and $\Delta u_{2,peak}$ is about 5 kPa for all simulated dissipation scenarios. The results for OCR = 4 show a strongly non-monotonic u_2 response where the difference between $\Delta u_{2,o}$ and $\Delta u_{2,peak}$ is about 130–150 kPa. This is consistent with published u_2 dissipation traces in varying OCR conditions, including those published by Chai et al. (2014), that show a stronger non-monotonic response as OCR increases.

The non-monotonic u_2 response for OCR = 4 is affected by k_h/k_v, where $\Delta u_{2,peak}$ decreases as the k_h/k_v ratio increases. Specifically, $\Delta u_{2,peak}$ with $k_h/k_v = 1$ is about 10% larger than $\Delta u_{2,peak}$ for $k_h/k_v = 10$. These results indicate that vertical Δu migration does affect the u_2 response, however, vertical Δu migration is likely not the driving mechanism of non-monotonic u_2 dissipation responses since vertical Δu migration is slightly suppressed for the $k_h/k_v = 10$ case compared to the isotropic case.

Dissipation rates do increase as k_h increases and k_v is kept constant, as is expected. However, increases in dissipation rate, represented by t_{50}, are less than the increase in k_h. t_{50} is the time to 50% dissipation from the Δu_1 or Δu_2 values at the start of the dissipation test and are directly related to the coefficient to consolidation in many common CPTu test interpretation methods (e.g., Teh and Houlsby, 1991; Agaiby and Mayne, 2018). Figure 5 plots the t_{50} values for both u_1 and u_2 dissipation from the results in Figure 4 versus model-assigned k_h values. For the non-monotonic u_2 responses for OCR = 4, the t_{50} is the time to reach 50% of the peak Δu from the time that the dissipation curve reaches its peak according to the Sully et al. (1999) correction. This t_{50} correction for the non-monotonic tests results in a very small change to t_{50} due to dissipation trends occurring over a log-time scale, and the results of this study are insensitive to this correction. The t_{50} results show that increases of k_h from $k_h/k_v = 1$ conditions do not result in directly proportional changes to t_{50} at either the u_1 or u_2 positions, indicating that u_1 and u_2 dissipation tests respond to both k_h and k_v.

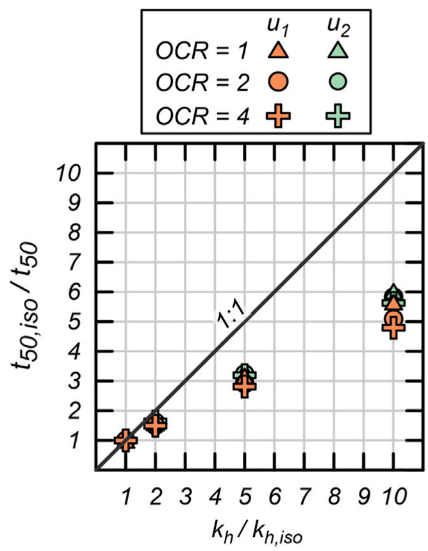

FIGURE 6
Change in t_{50} from CPTu dissipation as k_h/k_v changes showing that t_{50} is a response to both k_h and k_v.

The contribution of vertical Δu to reach t_{50} for isotropic conditions ($k_h = k_v$) is about 40%–44% for the u_2 response and 43%–51% for the u_1 response. These values are interpreted from Figure 6, which plots the ratio of t_{50} from $k_h = k_v = 10^{-7} m/s$ ($t_{50,iso}$) to the t_{50} for anisotropic conditions ($t_{50,iso}/t_{50}$) against k_h/k_v. The 1:1 line on Figure 6 represents where $t_{50,iso}/t_{50}$ would plot if k_h and k_v increased isotropically. The values of vertical Δu contribution are approximated by assuming that Δu is dominated by horizontal migration for the $k_h = 10k_v$ conditions. For example, with OCR = 1 the t_{50} for $k_h = 10k_v = 10^{-6}$ m/s is 40% smaller than the t_{50} would be for $k_h = k_v = 10^{-7}$ conditions at the u_2 position, and 44% at the u_1 position. The contribution of vertical Δu increases as OCR increases; these increases are addressed in detail in the

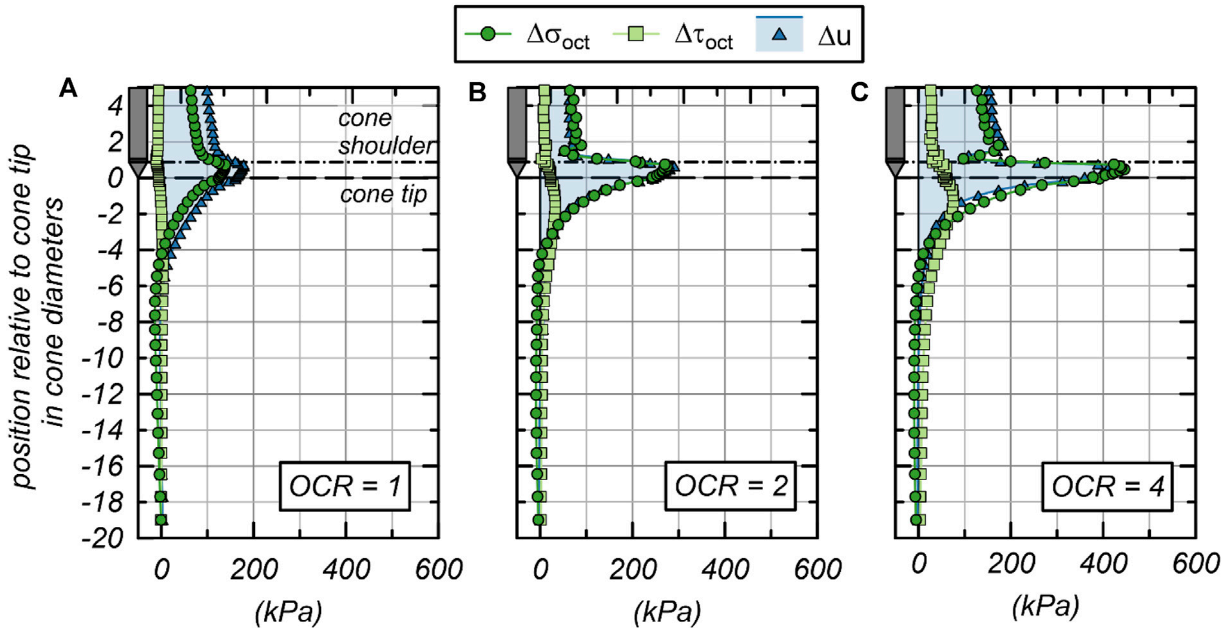

FIGURE 7
Change in octahedral stresses, shear stresses, and pore pressures relative to initial conditions along the penetrating cone path for steady state undrained penetration in **(A)** OCR = 1, **(B)** OCR = 2, and **(C)** OCR = 4 clay.

discussion section below. The slightly greater contribution of vertical Δu at the u_1 position is attributed to the gradients in the initial Δu distribution during undrained cone penetration, which are discussed in the next section.

3.2 Excess porewater pressure distribution during piezocone dissipation

The Δu distribution during undrained cone penetration and during dissipation is examined in this section. The distributions provide additional evidence that vertical Δu migration contributes to u_1 and u_2 dissipation responses and should be considered for dissipation test interpretation, and that non-monotonic test responses are primarily due to horizontal Δu migration.

The Δu field during undrained penetration is induced by a combination of changes in normal and shear stresses from initial static conditions that are dependent on OCR (e.g., Burns and Mayne, 1998; Krage and DeJong, 2016). This section examines how changes in octahedral normal total stress ($\Delta\sigma_{oct}$) and octahedral shear stress ($\Delta\tau_{oct}$) relate to Δu for the three initial conditions with OCR = 1, 2, and 4.

Figure 7 plots the steady-state undrained penetration profiles of $\Delta\sigma_{oct}$, $\Delta\tau_{oct}$, and Δu as soil transitions from initial conditions ahead of the penetrating cone, to the penetrating cone face, and then to the cone shaft. These profiles show that Δu strongly relates to $\Delta\sigma_{oct}$, and that large $\Delta\sigma_{oct}$ unloading from the cone face to the cone shoulder corresponds to differences between u_1 and u_2. There is some contribution to Δu from $\Delta\tau_{oct}$ depending on OCR, though it is less than the contribution of $\Delta\sigma_{oct}$. For OCR = 1, Δu = 159 kPa and $\Delta\sigma_{oct}$ = 111 kPa at the u_2 position and Δu = 172 kPa and $\Delta\sigma_{oct}$ = 132 at the u_1 position; therefore, $\Delta\tau_{oct}$ causes an overall increase in Δu. With OCR = 2, Δu = 172 kPa and $\Delta\sigma_{oct}$ = 165 kPa at the u_2 position and Δu = 262 kPa and $\Delta\sigma_{oct}$ = 261 kPa; therefore, there is minimal change in Δu due to $\Delta\tau_{oct}$, which is consistent with constitutive behavior of OCR = 2 clay in shear loading. For OCR = 4, Δu = 81 kPa and $\Delta\sigma_{oct}$ = 148 kPa at with u_2 position and Δu = 407 kPa and $\Delta\sigma_{oct}$ = 422 kPa; there is a reduction in Δu due to $\Delta\tau_{oct}$ up to 2.5 cone diameters ahead of the cone tip, but the reduction is small compared to Δu induced by $\Delta\sigma_{oct}$. Figure 7 also shows that the u_2 position is in a transition area between the cone face and cone shaft; therefore, u_2 may not fully reflect loading conditions on either the cone face or cone shaft. This effect of this transition between the cone tip and cone shaft on the u_2 dissipation response is examined in Lim et al. (2019).

The decrease in Δu from the cone face to the cone shoulder in Figure 7 possibly drives some vertical Δu migration during dissipation from the cone tip to the cone shoulder. As OCR increases, the difference between Δu_1 and Δu_2 increases which causes a larger Δu gradient between the cone face and cone shoulder. Between the u_1 and u_2 positions, Δu reduces by about 8% for OCR = 1 from 172 kPa at u_1 to 159 kPa at u_2; 34% for OCR = 2 from 262 kPa at u_1 to 172 kPa at u_2; and 80% for OCR = 4 from 407 kPa at u_1 to 81 kPa at u_2. This may relate to a more strongly non-monotonic u_2 dissipation response as OCR increases. Similarly, the Δu gradient downward from the cone tip increases as OCR increases, which is consistent with the larger role of vertical Δu migration at the u_1 position and as OCR increases.

Radial Δu distributions at steady state penetration conditions (t = 0) and during simulated dissipation from u_2 and u_1 positions are plotted in Figure 8. Distributions for $k_h = k_v = 10^{-6}\, m/s$ and $k_h = 10k_v = 10^{-6}$ m/s are presented to compare the soil response with isotropic and strongly anisotropic k. Distributions are plotted for times relative to t_{50} determined at the u_2 position for

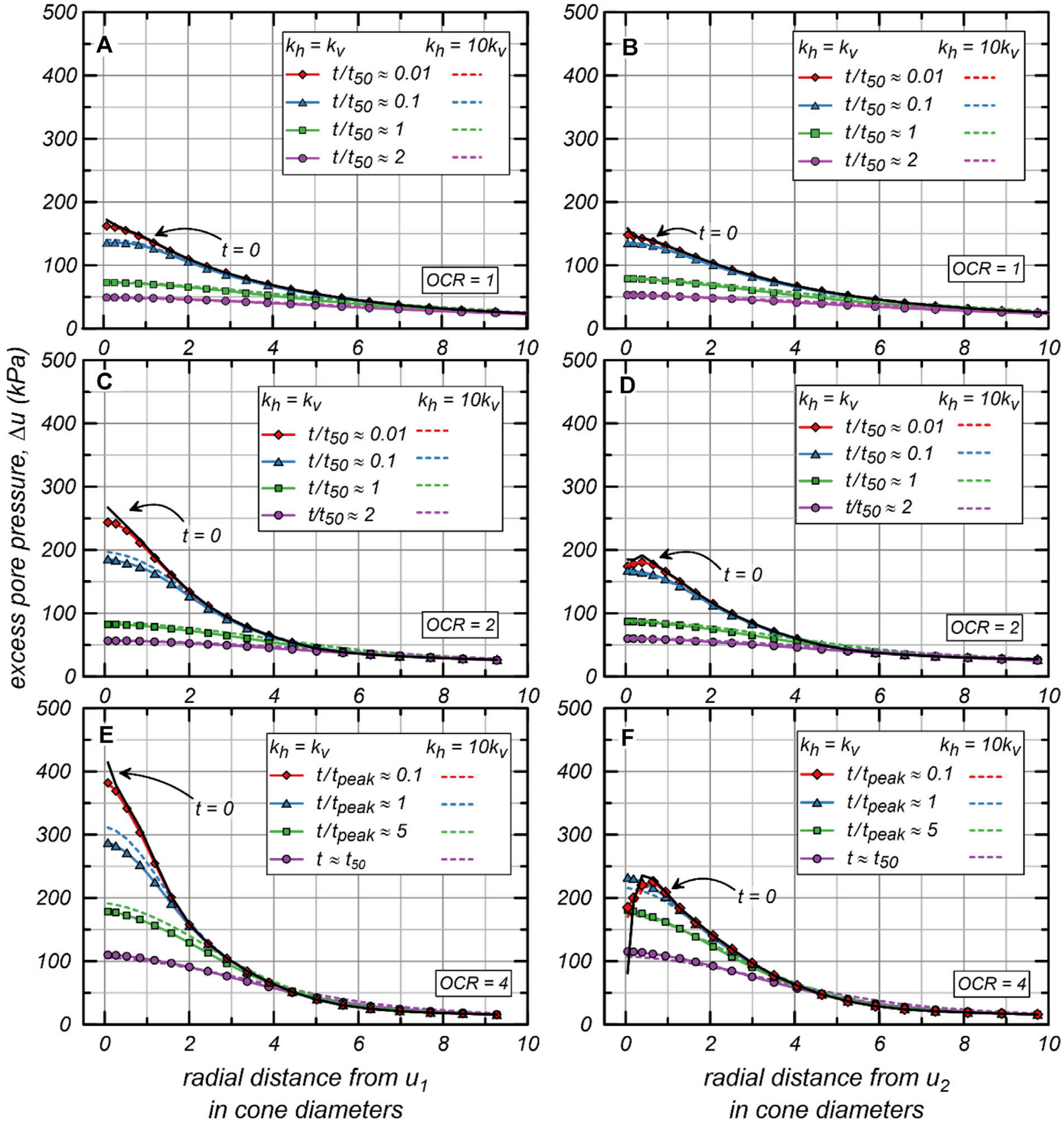

FIGURE 8
Radial distributions of Δu from u_1 **(A–C)** and u_2 **(D–F)** during simulated dissipation for k_h/k_v = 1 and 10.

OCR = 1 and 2 and t_{peak} for the strongly non-monotonic response of OCR = 4. This provides insight into how soil response differs between monotonic and non-monotonic dissipation tests. Since the response of OCR = 2 is slightly non-monotonic, the distributions at t_{peak} are not considered for radial distributions. Distributions are plotted over a radial distance of 10 cone diameters from the simulated penetrometer, which is smaller than the influence zone but allowed examination of conditions near the penetrometer. For all OCR values, the initial distributions from the u_1 position are monotonic and remain so throughout dissipation (Figures 8A, C, E). The radial distribution from the u_2 position is initially monotonic and remains so throughout dissipation for OCR = 1 (Figure 8B). The radial Δu distribution from u_2 for OCR is initially slightly non-monotonic with Δu_2 = 172 kPa and the maximum Δu in the distribution equal to 192 kPa; the distribution becomes monotonic by $t = 0.1t_{50}$ for OCR = 2 (Figure 8D) with Δu_2 = 167 kPa for both k_h/k_v = 1 and 10. The radial Δ u distribution from u_2 is initially non-monotonic for OCR = 4 with Δu_2 = 81 kPa and the maximum Δu equal to 235 kPa (Figure 8F); the distribution becomes monotonic by $t = t_{peak}$ at which time Δu_2 = 232 kPa for $k_h = k_v$ and 216 kPa for $k_h = 10k_v$.

The results in Figure 8 show that there are small differences in radial Δu distributions between the $k_h = k_v$ and $k_h = 10k_v$ cases that are attributable to different contributions of vertical and horizontal

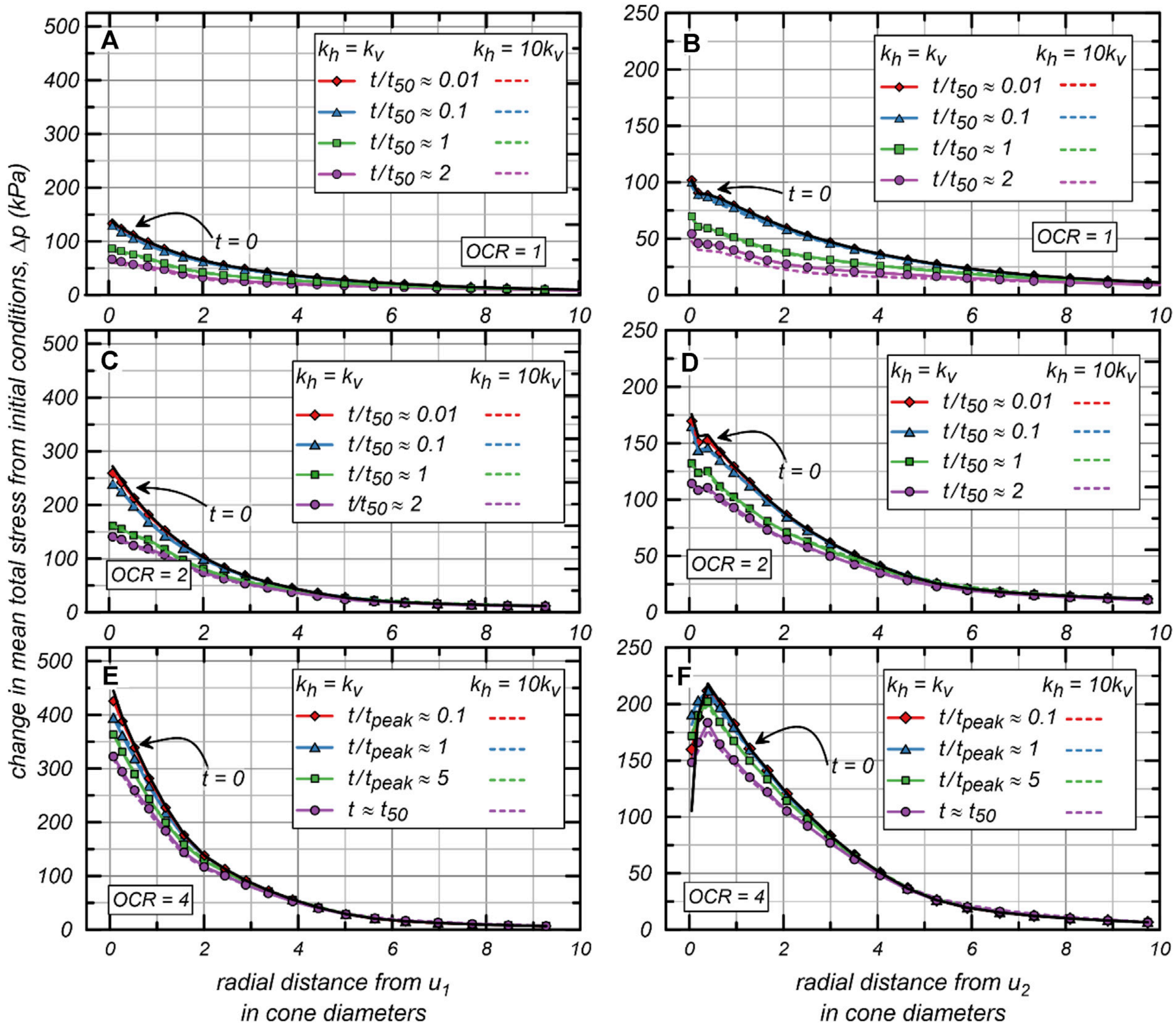

FIGURE 9
Radial distributions of Δp from u_1 **(A–C)** and u_2 **(D–F)** during simulated dissipation for k_h/k_v = 1 and 10.

Δu migration. For OCR = 1 and 2, Δu_1 at $t = t_{50}$ is slightly larger at the cone face for the $k_h = 10k_v$ case (Δu_1 = 74 kPa and 86 kPa for OCR = 1 and 2, respectively) than the $k_h = k_v$ case (Δu_1 = 72 kPa and 82 kPa for OCR = 1 and 2, respectively); this is likely due to more vertical Δu dissipation leading to lower Δu_1 for the isotropic k case.

The OCR = 4 radial Δu distributions for $t = 0.1t_{peak}$, $t = t_{peak}$, $t = 5t_{peak}$, and $t = t_{50}$ are shown in Figures 8E, F. These distributions indicate that both radial Δu migration towards the u_2 position and vertical Δu migration from the cone face to the cone shoulder contribute to the simulated non-monotonic u_2 responses. The initial Δu distribution from the u_2 position is non-monotonic with the maximum Δu value of 235 kPa generated at about 0.6 cone diameters from u_2 position. The distributions remain non-monotonic until $t = t_{peak}$, indicating that some radial Δu redistribution towards the u_2 position contributes to the non-monotonic response. At $t = t_{peak}$ and $t = 5t_{peak}$ there are notable differences between the $k_h = k_v$ and $k_h = 10k_v$ cases, specifically, Δu adjacent to the cone is larger at u_2 and smaller at u_1 for the $k_h = k_v$ case (Δu_2 = 232 kPa and Δu_1 = 287 kPa at $t = t_{peak}$; Δu_2 = 181 kPa and Δu_1 = 179 at $t = 5t_{peak}$) compared to the $k_h = 10k_v$ case (Δu_2 = 216 kPa and Δu_1 = 311 kPa at $t = t_{peak}$; Δu_2 = 174 kPa and Δu_1 = 191 at $t = 5t_{peak}$), which may be due to a larger contribution of vertical Δu migration from the cone face to the cone shoulder for the isotropic case than for the anisotropic case.

3.3 Mean total and effective stress during piezocone dissipation

Radial distributions of change in mean total stress from initial conditions (Δp) (plotted in Figure 9) show dependence on OCR and little dependence on k_h/k_v. Mean total stress (p) unloading between the cone face and cone shoulder is evident in radial distributions and the magnitude of p unloading increases as OCR increases, which is consistent with $\Delta\sigma_{oct}$ distributions in Figure 7. For OCR = 1 and OCR = 2, notable changes in Δp distribution do not occur until $t/t_{50} > 0.1$; at $t = t_{50}$ and $t = 2t_{50}$ there is an overall decrease in Δp as soil consolidates around the penetrometer. Between the initial conditions and $t = 2t_{50}$ for OCR = 1,

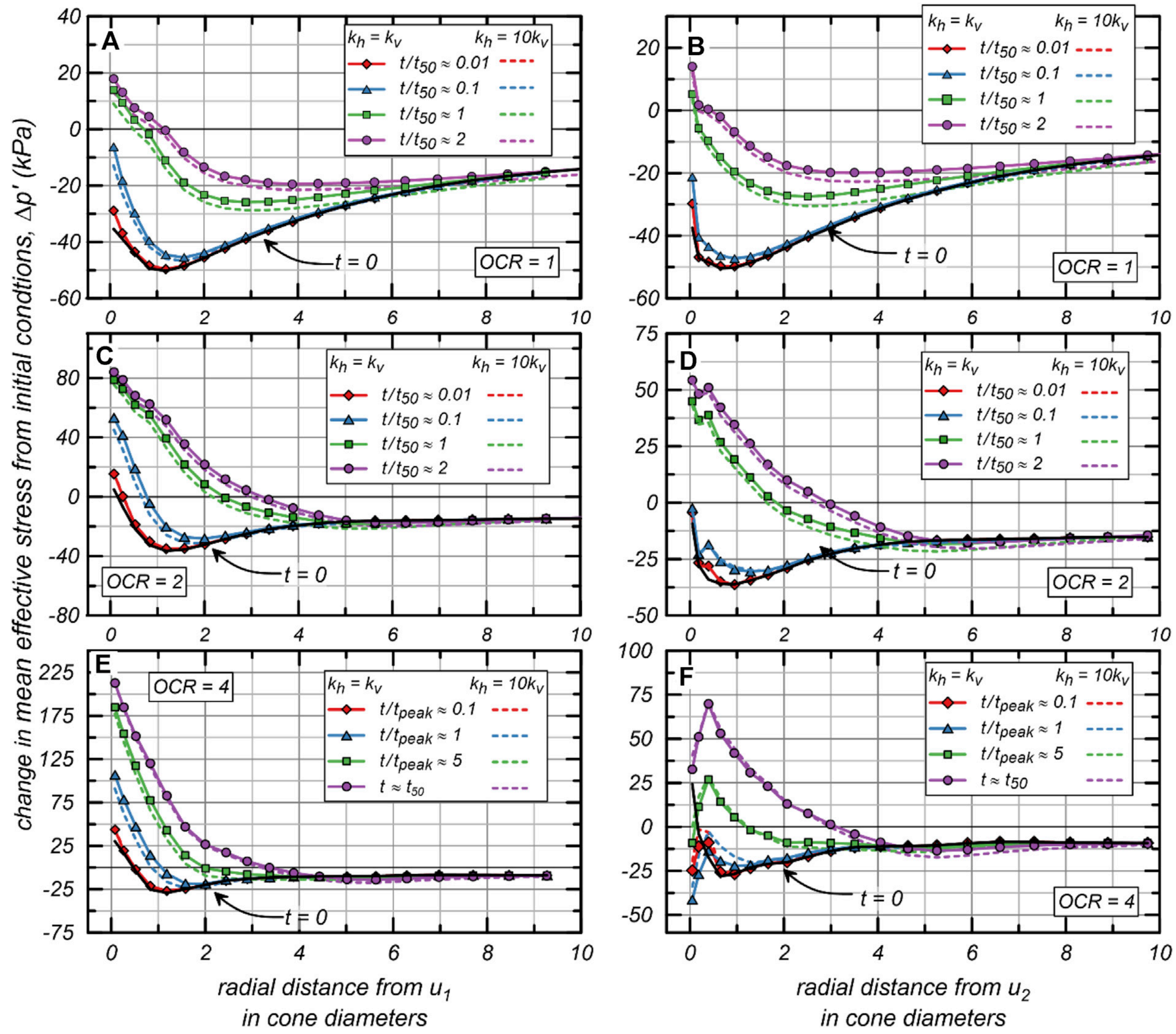

FIGURE 10
Radial distributions of $\Delta p'$ from u_1 (A–C) u_2 (D–F) during simulated dissipation for k_h/k_v = 1 and 10.

Δp adjacent to the cone decreases from 101 kPa to 52 kPa at u_2 and from 137 kPa to 67 kPa at u_1. Between the initial conditions and $t = 2t_{50}$ for OCR = 2, Δp adjacent to the cone decreases from 176 kPa to 114 kPa at u_2 and from 272 kPa to 141 kPa at u_1. For OCR = 4, changes in Δp distribution primarily occur when $t > t_{peak}$. The radial distributions from u_2 for OCR = 4 (Figure 9F) are non-monotonic throughout dissipation with the distribution becoming less non-monotonic during dissipation. The initial Δp at the u_2 position is 105 kPa with a maximum value of 248 in the radial distribution, by $t = t_{50}$ Δp at the u_2 position is 148 kPa with a maximum value of 184 in the radial distribution. The non-monotonic distribution may be due to combined unloading from the cone face to cone shoulder and friction at the cone-soil interface. At the u_1 position for OCR = 1, the initial Δp is 445 kPa and decreases to 323 kPa by $t = t_{50}$.

The radial distributions of change in mean effective stress from initial conditions ($\Delta p'$) are plotted in Figure 10; these distributions are directly related to the distributions in Δu and Δp in Figures 8, 9, respectively. Therefore, the $\Delta p'$ values during dissipation are affected by k_h/k_v in the same way that Δu distributions are affected by k_h/k_v. Overall, radial $\Delta p'$ distributions increase during consolidation around the piezocone and result in larger mean effective stress (p') near the cone than the initial conditions, this is consistent with loading from the penetrometer transferring from the pore fluid to the soil skeleton during dissipation and consolidation. This effect is stronger with increasing OCR, which leads to larger $\Delta p'$ as OCR increases. For instance, the maximum $\Delta p'$ from the u_2 position at $t = t_{50}$ is 5.2 kPa for OCR = 1, 45 kPa for OCR = 2, and 70 kPa for OCR = 4; and the maximum $\Delta p'$ from the u_1 position at $t = t_{50}$ is 14 kPa for OCR = 1, 79 kPa for OCR = 2, and 213 kPa for OCR = 4. p' at some distances remains lower than the initial conditions for all OCRs; however, it is expected that p' continues to increase as dissipation continues past $t = t_{50}$.

3.4 Volumetric strain during piezocone dissipation

The radial ε_v distributions, plotted in Figure 11, show responses that primarily depend on OCR, with little difference attributed to

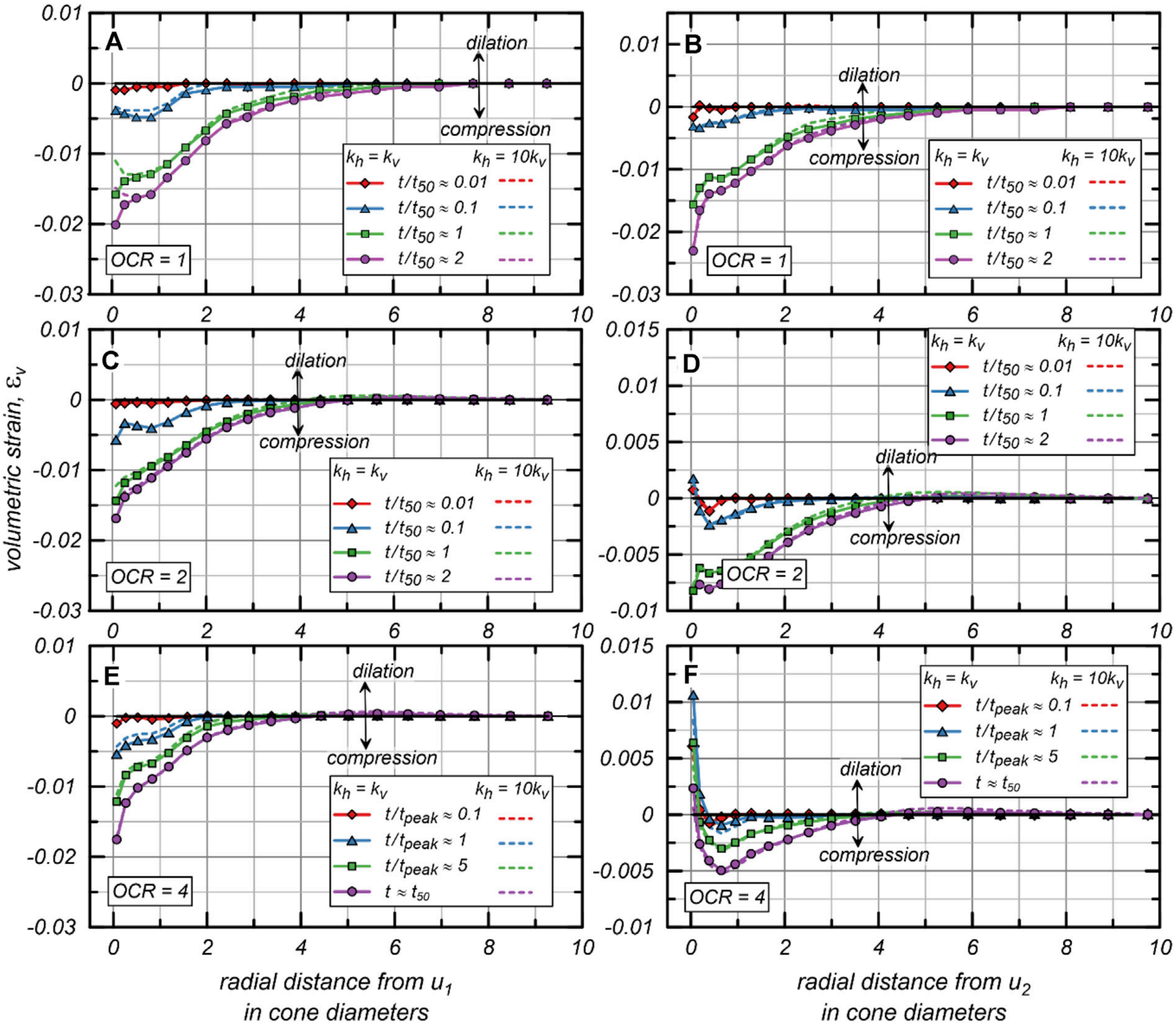

FIGURE 11
Radial distributions of ε_v from u_1 **(A–C)** and u_2 **(D–F)** during simulated dissipation for k_h/k_v = 1 and 10.

k_h/k_v. Since dissipation tests were simulated following undrained penetration conditions, the ε_v distribution at $t = 0$ is zero for all cases. Distributions from the u_1 position for all OCRs show similar contractive ε_v values adjacent to the cone face at $t = t_{50}$. The similar values of ε_v at $t = t_{50}$ near the u_1 position for all OCRs (−0.016 for OCR = 1, −0.014 for OCR = 2, and = 0.017 for OCR = 4) is attributed to compensating effects of larger Δu and greater soil stiffness as OCR increases. The simulated ε_v response for OCR = 1 is contractive from the u_2 position; there is little change in ε_v at $t/t_{50} = 0.01$, and then ε_v develops to −0.003 adjacent to the cone by $t/t_{50} = 0.1$ and −0.016 for $t = t_{50}$. This is consistent with the Δu response for OCR = 1 in Figure 9 where there is little change in Δu distributions when t is less than $t/t_{50} = 0.1$. For both the OCR = 2 and OCR = 4 simulations, the simulated ε_v response close to the u_2 position is initially dilative with $\varepsilon_v = 0.0017$ for OCR = 2 at $t = 0.1t_{50}$ and $\varepsilon_v = 0.011$ for OCR = 4 at $t = t_{peak}$, which is consistent with the slightly non-monotonic response of OCR = 2, the strongly non-monotonic response for OCR = 4, and supports some radial Δu re-distribution towards the u_2 position at early times (Figures 8D, F). Dilation dominates the response adjacent to the u_2 position for OCR = 4 throughout dissipation, however the dilation response is limited to less than 0.5 cone diameters from the u_2 position and at further distances the response is compressive. The role of k anisotropy on the ε_v response is small and is consistent with the small differences in Δu distributions between the $k_h = k_v$ and $k_h = 10k_v$ cases.

4 Discussion

Numerical simulations of CPTu dissipation using large deformation methods allow investigation of Δu generation and dissipation as a system response to loading conditions imposed by the penetration cone, clay behavior, and hydraulic properties of the soil. This numerical study shows that at both the u_1 and u_2 positions, and for OCR 1, 2, and 4, vertical Δu does have a contribution to the dissipation response for soils with isotropic or slightly anisotropic hydraulic conductivity. This finding is contrary to early CPTu dissipation test analysis, which assumed

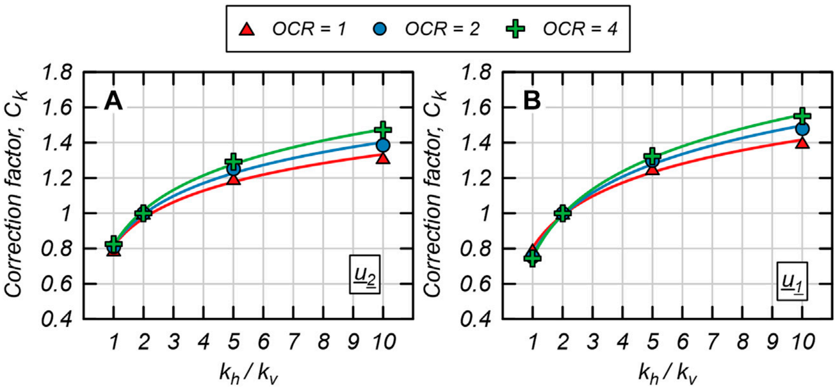

FIGURE 12
Correction factor (C_k) to estimate c_h from CPTu dissipation test interpreted c_{vh}.

that due to natural soil anisotropy and induced gradients, Δu was dominant in the horizontal direction. However, this study supports the assertion by Agaiby and Mayne (2018) that the coefficient of consolidation estimated from CPTu tests should be represented as c_{vh} to reflect dissipation in both the horizontal and vertical directions.

Based on the simulated t_{50} values in Figure 5, corrections to c_{vh} to estimate c_h are develop in Figure 12 and presented below, where:

$$c_h \approx C_k{}^* c_{vh} \quad (2)$$

$$C_k = A \ln\left(\frac{k_h}{k_v}\right) + B \quad (3)$$

C_k is a suggested correction factor to account for k_h/k_v when interpreting c_h. The factors A and B are fit to the simulated results for u_1 and u_2 dissipation and OCR = 1, 2, and 4. The suggested values of A and B at these OCR values are summarized in Table 1. For OCR values between those listed in Table 1, it would be reasonable to interpolate between A and B values.

The C_k approach is intended for use with CPTu interpretation methods that are based on estimation of t_{50} (e.g., Teh and Houlsby, 1991; Agaiby and Mayne, 2018) and for normal clays with OCR 1 to 4. Use of this approach outside of these conditions and soil type requires further study and validation.

The C_k values are based on k_h/k_v, which would be estimated from either hydrogeologic studies, laboratory testing, or knowledge of the depositional environment (e.g., Leroueil and Jamiolkowski 1991). $k_h = 2k_v$ represents the assumed baseline anisotropy conditions from which CPTu dissipation test interpretation methods were initially developed and validated, and therefore little adjustment is needed (i.e., $c_h = 2c_v \approx c_{vh}$). This assumption is based on Teh and Houlsby (1991) who report little difference between dissipation curves once $k_h > 2k_v$; Sully et al. (1999) who evaluated the proposed non-monotonic u_2 test correction to t_{50} with soils with k_h/k_v from 1 to 3 (i.e., isotropic to slightly anisotropic). As k_h/k_v increases, t_{50} at the u_1 and u_2 positions will increase since there is limited Δu dissipation in the vertical direction, and the interpreted c_{vh} will decrease. Therefore, as the soil becomes more hydraulically anisotropic, C_k increases to reflect the decreasing contribution of vertical Δu.

C_k differs slightly between u_1 and u_2 CPTu dissipation curves, as shown in Figures 12A, B, respectively, and OCR values. The C_k range is slightly larger for u_1 dissipation, ranging from 0.75 to 1.55, compared to u_2 dissipation, which ranges from 0.79 to 1.47. This is consistent with the previous observation that vertical Δu dissipation is more dominant in the cone tip area due to hydraulic gradients vertically down from the cone tip and between the cone tip and the cone shaft. The range of C_k also increases as OCR increases, which indicates that vertical Δu becomes more important as OCR increases, potentially due to increasing Δu gradients.

The interpretation of c_{vh} and c_h from the simulated dissipation curves (termed $c_{vh,interpreted}$ and $c_{h,interpreted}$, respectively) are shown in Figure 13. The $c_{vh,interpreted}$ values are found from the simulated t_{50} (Figure 5) using the Teh and Houlsby (1991) interpretation approach:

$$c_{vh} = \frac{T^*_{50} r^2 I_r^{0.5}}{t_{50}} \quad (4)$$

T^*_{50} is the time factor for 50% dissipation; at the u_1 position it is equal to 0.069 and at the u_2 position it is equal to 0.245. r is the cone radius, which was 18 cm in the model. I_r is the soil rigidity index, which is the ratio of soil shear modulus to undrained shear strength. The I_r values are 115, 148, and 111 for OCR = 1, 2, and 4, respectively. The I_r values were determined from single element undrained isotropic consolidation triaxial compression simulations. Although Teh and Houlsby (1991) designate the interpretation to be c_h, this study uses c_{vh} in Eq. 4 following the confirmation that vertical Δu contributes to the CPTu dissipation response.

The $c_{vh,interpreted}$ values at the u_1 and u_2 positions are compared to the model-assigned c_h values ($c_{h,model}$) in Figures 13A, B, respectively. There is generally strong agreement between $c_{vh,interpreted}$ and $c_{h,model}$ across OCR and k_h/k_v values, providing further support that CPTu dissipation is reasonably captured by the cone penetration and dissipation model, with general scatter around the 1:1 lines. The C_k values are applied to $c_{vh,interpreted}$ values in Figures 13C, D with Eq. 2 to estimate $c_{h,interpreted}$. As expected, there is less scatter for Figures 13C, D than in Figures 13A, B when C_k is not applied.

TABLE 1 Factors for use with Eq. 3 to estimate C_k

	u_1			u_2		
	OCR = 1	OCR = 2	OCR = 4	OCR = 1	OCR = 2	OCR = 4
A	0.265	0.316	0.351	0.225	0.254	0.282
B	0.805	0.769	0.750	0.816	0.819	0.816

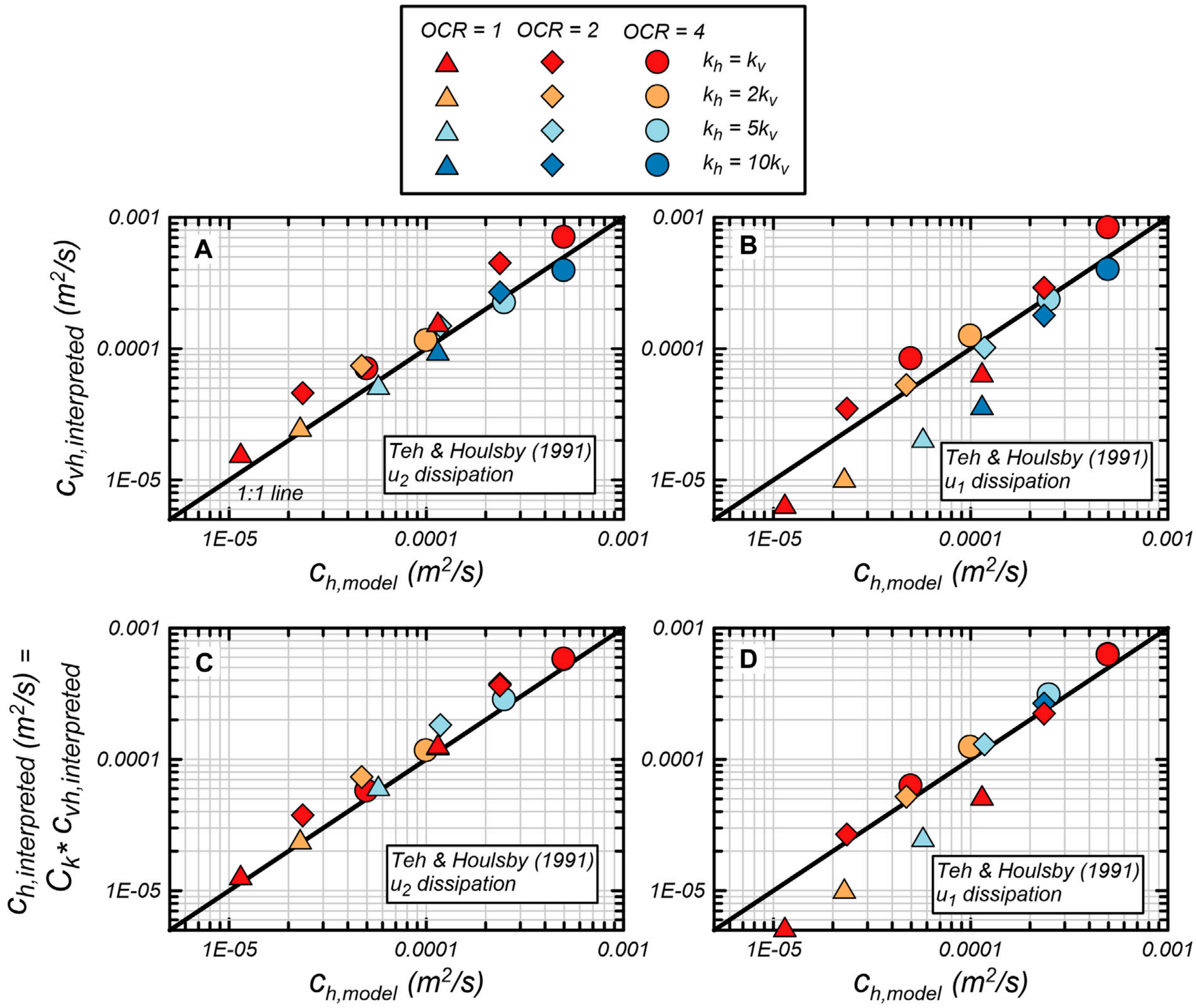

FIGURE 13
Comparison of model assigned c_h and interpretation of c_{vh} or c_h from simulated CPTu dissipation tests: **(A)** u_2-interpreted c_{vh}, **(B)** u_1-interpreted c_{vh}, **(C)** u_2-interpreted c_h using C_k, and **(D)** u_1-interpreted c_h using C_k.

5 Conclusion

CPTu dissipation simulations were performed in saturated clay with a direct axisymmetric cone penetration model to examine test interpretation methods, and how dissipation is affected by OCR and k_h/k_v. Simulations were performed with the MIT-S1 constitutive model calibrated for BBC with OCR = 1, 2, and 4. The simulated u_1 dissipation tests showed monotonic responses for all OCR values. The simulated u_2 dissipation tests showed a monotonic response for OCR = 1, a slightly non-monotonic response for OCR = 2, and a strongly non-monotonic response for OCR = 4.

This study examined simulated Δu migration during dissipation. The results showed that Δu migration occurs in both the vertical and radial directions. Contribution of vertical Δu migration to CPTu dissipation tests is shown by 1) increased time to t_{50} at both the u_1 and u_2 position when k_v is reduced but k_h remains the same and 2) reduced $\Delta u_{2,peak}$ for non-monotonic dissipation tests as k_h/k_v increases. Vertical Δu migration may be driven by a gradient between the cone face and cone shaft that is induced by normal stress unloading and shear stress. This gradient was present for all OCR simulations and increased as OCR increased, which is notable since higher OCR is associated with stronger non-monotonic u_2 dissipation responses. Non-monotonic u_2 responses were also associated with initially non-monotonic radial Δu distribution from the u_2 position, indicating that radial Δu migration may also contribute to non-monotonic u_2 dissipation responses. Future research efforts will map Δu migration around the piezocone to relate migration to initial Δu distribution and recorded dissipation curves.

The role of hydraulic conductivity anisotropy and vertical Δu migration is incorporated into dissipation test interpretation with a correction factor, termed C_k, based on prior knowledge of k_h/k_v. The correction factor is applied to the c_{vh} value interpreted from CPTu dissipation tests to estimate c_h. The correction factor is based on changes in t_{50} with hydraulic conductivity anisotropy, and therefore, is appropriate for use with t_{50}-based c_{vh} interpretation methods such as Teh and Houlsby (1991) or Agaiby and Mayne (2018) and for normal clays that are normally consolidated to moderately overconsolidated (i.e., OCR = 1–4).

Data availability statement

The raw data supporting the conclusion of this article will be made available by the authors, without undue reservation.

Author contributions

DM: Investigation, Methodology, Supervision, Writing–original draft. AH: Data curation, Investigation, Writing–review and editing. JD: Conceptualization, Writing–review and editing.

Funding

The author(s) declare that financial support was received for the research, authorship, and/or publication of this article. Funding for this research was provided by the National Science Foundation (award CMMI-1927557). Any opinions, findings, and conclusions or recommendations expressed in this material are those of the authors and do not necessarily reflect the views of the agency.

Conflict of interest

The authors declare that the research was conducted in the absence of any commercial or financial relationships that could be construed as a potential conflict of interest.

Publisher's note

All claims expressed in this article are solely those of the authors and do not necessarily represent those of their affiliated organizations, or those of the publisher, the editors and the reviewers. Any product that may be evaluated in this article, or claim that may be made by its manufacturer, is not guaranteed or endorsed by the publisher.

References

Abu-Farsakh, M., Tumay, M., and Voyiadjis, G. (2003). Numerical parametric study of piezocone penetration test in clays. *Int. J. Geomech.* 3 (2), 170–181.

Agaiby, S. S., and Mayne, P. W. (2018). Interpretation of piezocone penetration and dissipation tests in sensitive leda clay at gloucester test site. *Can. Geotech. J.* 55, 1781–1794. doi:10.1139/cgj-2017-0388

Ansari, Y., Merifield, R., and Sheng, D. (2014). A piezocone dissipation test interpretation method for hydraulic conductivity of soft clays. *Soils Found.* 54 (6), 1104–1116. doi:10.1016/j.sandf.2014.11.006

Baligh, M. M., and Levadoux, J. N. (1986). Consolidation after undrained piezocone penetration. II: interpretation. *J. Geotech. Eng.* 112 (7), 727–745. doi:10.1061/(asce)0733-9410(1986)112:7(727)

Burns, S., and Mayne, P. (1998). Monotonic and dilatory pore-pressure decay during piezocone tests in clay. *Can. Geotech. J.* 35 (6), 1063–1073. doi:10.1139/t98-062

Ceccato, F., and Simonini, P. (2016). Numerical study of partially drained penetration and pore pressure dissipation in piezocone test. *Acta Geotech.* 12, 195–209. doi:10.1007/s11440-016-0448-6

Chai, J., Sheng, D., Carter, J. P., and Zhu, H. (2012). Coefficient of consolidation from non-standard piezocone dissipation curves. *Comput. Geotechnics* 41, 13–22. doi:10.1016/j.compgeo.2011.11.005

Chai, J. C., Hossain, M. J., Carter, J., and Shen, S. L. (2014). Cone penetration-induced pore pressure distribution and dissipation. *Comput. Geotechnics* 57, 105–113. doi:10.1016/j.compgeo.2014.01.008

Chen, B. S. Y., and Mayne, P. W. (1994) *Profiling the OCR of clays by piezocone tests.* Rep. No. CEEGEO-94 1.

DeJong, J. T., and Randolph, M. (2012). Influence of partial consolidation during cone penetration on estimated soil behavior type and pore pressure dissipation measurements. *J. Geotech. Geoenviron.* 138 (7), 777–788. doi:10.1061/(asce)gt.1943-5606.0000646

Deng, S., Zhang, Y., Han, J., Tian, Z., and Liu, T. (2023). An analytical study on penetration and pore pressure dissipation of piezocone test in typical normally and over-consolidated silty clays. *Appl. Sci.* 13, 3797. doi:10.3390/app13063797

Dunn, R. J., and Mitchell, J. K. (1984). Fluid conductivity testing of fine-grained soils. *J. Geotech. Eng.* 110 (11), 1648–1665. doi:10.1061/(asce)0733-9410(1984)110:11(1648)

Finke, K. A., Mayne, P. W., and Klopp, R. A. (2001). Piezocone penetration testing in Atlantic Piedmont residuum. *J. Geotech. Geoenviron.* 127 (1), 48–54. doi:10.1061/(asce)1090-0241(2001)127:1(48)

House, R. D. (2012). "A comparison of the behavior of intact and resedimented Boston blue clay (BBC)," (Cambridge: Department of Civil and Environmental Engineering, Massachusetts Institute of Technology). PhD Thesis.

Imre, E., Rózsa, P., Bates, L., and Fityus, S. (2010). Evaluation of monotonic and non-monotonic dissipation test results. *Comput. Geotechnics* 37, 885–904. doi:10.1016/j.compgeo.2010.07.008

Itasca (2016) *FLAC version 8.0.* Minneapolis, Minnesota: Itasca Consulting Group Inc.

Jaeger, R. A. (2012). "Numerical and experimental study on cone penetration in sands and intermediate soils," (Davis: Department of Civil and Environmental Engineering, University of California). PhD Thesis.

Krage, C. P., and DeJong, J. T. (2016). Influence of drainage conditions during cone penetration on the estimation of engineering properties and liquefaction potential of silty and sandy soils. *J. Geotech. Geoenviron.* 142 (11), 04016059. doi:10.1061/(asce)gt.1943-5606.0001543

Kulhawy, F. H., and Mayne, P. W. (1990). "Manual on estimating soil properties for foundation design," in *No. EPRI-EL-6800. Electric power research inst., palo alto, CA (USA)* (Ithaca, NY (USA): Cornell Univ.).

Leroueil, S., and Hight, D. W. (2003). Behaviour and properties of natural soils and soft rocks. *Characterisation and engineering properties of natural soils* 1, 29–254.

Lim, X. Y., Tan, S. A., and Phoon, K. (2019). Interpretation of horizontal permeability from piezocone dissipation tests in soft clays. *Comput. Geotechnics* 107, 189–200. doi:10.1016/j.compgeo.2018.12.001

Liu, K., Wang, D., and Zheng, J. (2022). Determination of the coefficient of consolidation by piezocone tests under partially drained conditions. *Geotechnique*, 1–11. doi:10.1680/jgeot.22.00064

Lu, Q., Randolph, M. F., Hu, Y., and Bugarski, I. C. (2004). A numerical study of cone penetration in clay. *Geotechnique* 54 (4), 257–267. doi:10.1680/geot.2004.54.4.257

Mahmoodzadeh, H., Randolph, M. F., and Wang, D. (2014). Numerical simulation of piezocone dissipation test in clays. *Geotechnique* 64 (8), 657–666. doi:10.1680/geot.14.p.011

Moug, D. M. (2017). "Axisymmetric cone penetration model for sands and clays," (Davis: Department of Civil and Environmental Engineering, University of California). PhD Thesis.

Moug, D. M., Boulanger, R. W., DeJong, J. T., and Jaeger, R. A. (2019). Axisymmetric simulations of cone penetration in saturated clay. *J. Geotech. Geoenviron.* 145 (4). doi:10.1061/(ASCE)GT.1943-5606.0002024

Pember, R., and Anderson, R. (2001). Comparison of direct Eulerian Godunov and Lagrange plus remap artificial viscosity schemes. In 15th AIAA Computational Fluid Dynamics Conference, 2644.

Pestana, J. M., and Whittle, A. J. (1999). Formulation of a unified constitutive model for clays and sands. *Int. J. Numer. Anal. Meth. Geomech.* 23 (12), 1215–1243. doi:10.1002/(sici)1096-9853(199910)23:12<1215::aid-nag29>3.0.co;2-f

Pestana, J. M., Whittle, A. J., and Gens, A. (2002). Evaluation of a constitutive model for clays and sands: Part II – clay behaviour. *Int. J. Numer. Anal. Mater. Geomech.* 26 (11), 1123–1146. doi:10.1002/nag.238

Sully, J. P., Robertson, P. K., Campanella, R. G., and Woeller, D. J. (1999). An approach to evaluation of field CPTU dissipation data in overconsolidated fine-grained soils. *Can. Geotech. J.* 36 (2), 369–381. doi:10.1139/cgj-36-2-369

Taylor, D. W. (1948) *Fundamentals of soil mechanics.* New York: John Wiley and Sons.

Teh, C., and Houlsby, G. (1991). An analytical study of the cone penetration test in clay. *Geotechnique* 41 (1), 17–34. doi:10.1680/geot.1991.41.1.17

Tsegaye, A. B. (2021). "Consolidation coefficient from cone penetration-based dissipation tests," in Proceedings of the 6th International Conference on Geotechnical and Geophysical Site Characterization, Budapest, Hungary, 07-09-2020 to 11-09-2020.